Title

Congenital heart disease assessment with 4D flow MRI.

Journal

Journal of magnetic resonance imaging : JMRI, 42(4)

ISSN

1053-1807

Authors

Vasanawala, Shreyas S

Hanneman, Kate

Alley, Marcus T

et al.

Publication Date

2015-10-01

DOI

10.1002/jmri.24856

Peer reviewed

Congenital Heart Disease Assessment With 4D Flow MRI

Shreyas S. Vasanawala, MD, PhD,[1]* Kate Hanneman, MD,[2]
Marcus T. Alley, PhD,[1] and Albert Hsiao, MD, PhD

With improvements in surgical and medical management, patients with congenital heart disease (CHD) are often living well into adulthood. MRI provides critical data for diagnosis and monitoring of these patients, yielding information on cardiac anatomy, blood flow, and cardiac function. Though historically these exams have been complex and lengthy, four-dimensional (4D) flow is emerging as a single fast technique for comprehensive assessment of CHD. The 4D flow consists of a volumetric time-resolved acquisition that is gated to the cardiac cycle, providing a time-varying vector field of blood flow as well as registered anatomic images. In this article, we provide an overview of MRI evaluation of congenital heart disease by means of example of three relatively common representative conditions: tetralogy of Fallot, aortic coarctation, and anomalous pulmonary venous drainage. Then 4D flow data acquisition, data correction, and postprocessing techniques are reviewed. We conclude with several examples that highlight the comprehensive nature of the evaluation of congenital heart disease with 4D flow.

J. MAGN. RESON. IMAGING 2015;00:000–000.

Congenital heart disease (CHD) is the most common type of birth defect, affecting nearly 1% of births per year.[1] Congenital heart defects are anatomic lesions that reflect abnormal size, connections or communications of the chambers of the heart or the arteries and veins adjacent to the heart. The physiologic consequences of congenital heart anomalies vary widely, ranging from an asymptomatic murmur detected only incidentally in adulthood, to severe cyanosis requiring urgent surgical intervention in the neonatal period. With improved surgical and medical management of these conditions, most children now survive into adulthood, and the prevalence of CHD has increased. MRI plays a critical role in the diagnosis and monitoring of these conditions.

Analysis of cardiac MRI exams usually consists of two components. One component consists of understanding the anatomical disorder; this is performed by a sequential segmental approach to CHD that was introduced approximately 25 years ago, and is now nearly universally used in the evaluation of CHD.[2] Here, cardiac anatomy is first assessed in three distinct segments—the atria, the ventricles, and the great vessels (aorta and pulmonary artery). The morphologic and anatomic features specific to each segment are assessed separately. Next, the relationships between the segments are assessed at the atrioventricular and ventriculoarterial levels. Finally, associated abnormalities in individual segments are evaluated. This approach is used to describe the wide range of different congenital cardiac defects and combinations of defects that may be encountered in clinical practice. Cardiac MRI is ideally suited to the detailed evaluation of cardiac anatomy underpinning this approach to CHD. The second component of analysis of cardiac MRI exams is determination of the physiologic consequences of the anatomical disorders. These consequences consist of abnormal blood flows, abnormal function of the ventricles, and abnormal function of the valves of the heart.

While an exhaustive description of the anatomical and physiologic considerations in all congenital heart diseases, as well as cardiac MRI techniques, is beyond the scope of this

View this article online at wileyonlinelibrary.com. DOI: 10.1002/jmri.24856

Received Oct 20, 2014, Accepted for publication Dec 18, 2014.

*Address reprint requests to: S.S.V., Department of Radiology, Stanford University, 725 Welch Road, Stanford, CA 94305. E-mail: shreyasv@stanford.edu

From the [1]Department of Radiology, Stanford University, Stanford, California, USA; and [2]Department of Radiology, University of California, San Diego, San Diego, California, USA

Contract grant number: P41 EB015881; Contract grant number: 2R01EB009690.

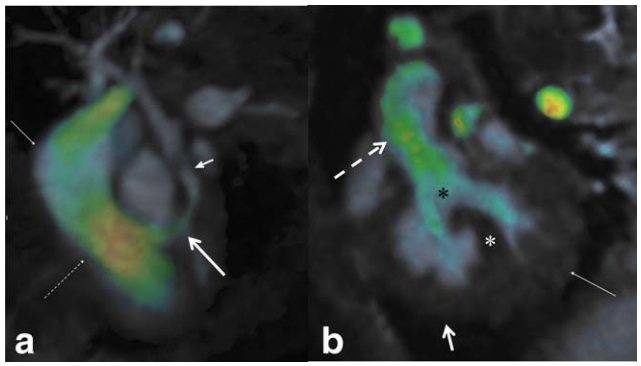

FIGURE 1: A 10-day-old with tetralogy of Fallot. a: Right-sided anatomic structures are right atrium (thin arrow), right ventricle (dashed arrow), right ventricular outflow tract (thick long arrow), and pulmonary artery (short arrow). Note the abnormally small right ventricular outflow tract. b: View showing the ventricular septal defect (black asterisk), which is a defect in the normal septum (white asterisk). The aorta (dashed arrow) overlies the defect. The right ventricular wall (short thick arrow) is abnormally thick. It is as thick as the left ventricular wall (thin arrow). The 4D flow acquisition with resolution 0.62 × 0.62 × 1.4 mm, TR 4.1 ms, TE 1.9 ms, venc 250 cm/s, temporal resolution 38 ms, bandwidth 83 KHz, accel eration 2.2 × 3, matrix 320 × 115 × 86, scan time 8:41, weight 3.2 kg, heart rate 115.

FIGURE 2: A 2-day-old with aortic coarctation. Note narrowing (arrow) of the aorta just beyond the aortic arch and resulting flow acceleration (reddish color overlay). The 4D flow scan parameters: resolution 0.75 × 0.75 × 1.4 mm, flip angle 15, TR 4 ms, TE 1.8 ms, temporal resolution 32 ms, venc 250 cm/s, BW 83 KHz, acceleration 2.4 × 2.4, matrix 320 × 157 × 112, and scan time 8:14.

article, we will first focus on the clinical management considerations of three relatively common and representative specific diseases. We then review 4D flow MRI acquisition and postprocessing techniques, and illustrate the comprehensive evaluation of 4D flow MRI exams in these three diseases.

Representative Congenital Heart Diseases

Repaired Tetralogy of Fallot

Tetralogy of Fallot (TOF) is one of the most common complex congenital heart defects requiring repair in infancy. The primary defect is an abnormality in the formation of the infundibular septum, which is a muscular wall between the two ventricles. This abnormality causes right ventricular outflow tract obstruction (RVOTO), i.e., blood cannot directly egress the right ventricle into the pulmonary artery. Rather, there is an abnormal communication between the left and right ventricles, termed a ventricular septal defect (VSD). The aorta is enlarged and overrides the ventricular septum. Finally, the right ventricle muscle bulk is often increased, termed right ventricular hypertrophy (RVH).[3] These characteristic features of TOF are illustrated in Figure 1. The mortality rate in untreated patients approaches 50% by the age of 6 years. However, with the introduction of modern surgical techniques, a dramatic 40% reduction in deaths associated with TOF was noted from 1979 to 2005,[4] with most patients now surviving well into adulthood.[5]

Contemporary surgical repair usually includes VSD closure and reduction of RVOTO.[6] While this has improved clinical outcomes, patients with repaired TOF (rTOF) require clinical and imaging follow-up to assess for common postsurgical complications. The most frequently encountered complication in patients with rTOF include pulmonary regurgitation (PR) and/or residual or recurrent pulmonary stenosis (PS). Chronic PR, when sufficiently severe, results in right ventricular dilation and arrhythmia. Pulmonary valve replacement is then required to prevent irreversible right ventricular failure. In practice, this is typically performed when patients develop clinical symptoms, when there are signs of developing right ventricular failure (RV end diastolic volume index >150 mL/m^2 and/or RV ejection fraction (EF) $<47\%$), among other factors.[7]

While MRI does not currently play a primary role in the initial diagnosis of TOF, it has emerged as the imaging method of choice in patients with rTOF, playing an integral role in postoperative follow-up and evaluation.[8,9] Typically, MRI is required beginning late in the first decade of life with continued imaging throughout life. Clinical goals of postoperative imaging include accurate quantification of PR and evaluation of biventricular size and function (including RVEF and RVEDV). Additional cardiac MRI findings that may be useful in risk stratification include assessment of RVOT aneurysm or akinesia, and quantification of the velocity and pressure gradient across the pulmonary valve in the setting of PS.[10]

Aortic Coarctation

Aortic coarctation is a short segment of narrowing of the aorta just beyond the origin of the arteries that supply the head and arms (Fig. 2). It is a common congenital cardiovascular defect with an estimated incidence of 1 in 2500

live births.[11] Coarctation of the aorta may occur as an isolated defect, or in association with other congenital lesions, notably bicuspid aortic valve (BAV).

Untreated aortic coarctation has a reported mortality rate of over 80% by 50 years of age, due to complications including aortic rupture and heart failure.[12] Early intervention with surgical—or more recently endovascular—repair has resulted in significantly reduced patient morbidity.[13,14] However, close follow-up, even after successful repair, is required as patients may experience complications both directly related to intervention and secondary to systemic arteriopathy.[12,15] Structural aortic complications include re-coarctation, aneurysm formation, and aortic rupture, which may be identified by MRI. Re-coarctation is associated with both recurrent hypertension and an increased mortality rate, and as such, accurate identification and characterization is imperative.[16]

Although diagnosis is often made by echocardiography, particularly in infancy, visualization of the distal aortic arch may be challenging in some situations. In these situations, often when coarctation is suspected beyond infancy, either CT angiography or MRI may be helpful. MRI has also emerged as the imaging option of choice in the setting of known or previously repaired coarctation, with its ability to provide both anatomic and hemodynamic information.[17,18] Anatomic assessment in patients with aortic coarctation includes assessment of the location and length of the narrowing, measurement of the smallest vessel diameter, evaluation of poststenotic dilation, and identification of collateral vessels. Hemodynamic assessment includes evaluation of the pressure gradient and maximum velocity across the coarctated segment, and evaluation of associated collateral flow, which typically indicates the presence of hemodynamically significant narrowing, likely requiring intervention.[19]

Anomalous Pulmonary Venous Return

Partial anomalous pulmonary venous return (PAPVR) is a relatively rare congenital defect where blood flow from some, but not all, of the pulmonary veins drain abnormally into a systemic vein or the right atrium. Thus, blood oxygenated by passage through the lungs recirculates back through the lungs instead of supplying oxygen to the rest of the body, constituting a left to right shunt. The most common form is a right upper pulmonary vein draining into the right atrium or the superior vena cava (SVC), and is frequently associated with a sinus venous atrial septal defect (ASD), usually located near the SVC orifice.[20] Though patients may come to attention prenatally or in infancy, patients with PAPVR are frequently asymptomatic and are often not diagnosed until adulthood.

Total anomalous pulmonary venous return (TAPVR) is even more rare, where the entirety of pulmonary venous drainage makes anomalous connections to the systemic venous circulation or right atrium. Four variants include supracardiac, in which drainage is to one of the innominate veins or the SVC; cardiac, in which blood drains directly into the coronary sinus or right atrium; infracardiac, with drainage to the portal or hepatic veins, and a mixed variant. An ASD or patent foramen ovale (PFO) must be present to allow oxygenated blood to flow to the left-side of the heart in order for an infant to survive with TAPVR. The management of TAPVR depends on the level of drainage and whether veins are obstructed. Infants with obstructed TAPVR are frequently symptomatic and are often surgically corrected early in life, with long-term postsurgical survival rates over 83%.[21]

Although transthoracic echocardiography is often performed as a first line imaging modality in patients with suspected anomalous pulmonary venous connections, MRI may provide additional noninvasive information if findings by echocardiography are uncertain.[22] MRI allows for noninvasive anatomic assessment of the number, origin, course and drainage of all pulmonary veins, including anomalous connections or obstruction, as well as evaluation of associated defects including ASDs. MRI also allows for quantification of RV size and function, and estimation of the shunt fraction. The ratio of pulmonary (Q_P) to systemic (Q_S) blood flow (Q_P/Q_S) is expected to be 1:1 in a normal physiologic setting. However, in PAPVR as with other left-to-right shunts, Q_P is greater than Q_S. Accurate evaluation of shunt size is important in patients with PAPVR as this may influence the decision to undergo surgical repair. In general, shunt fractions (Q_p/Q_s) that exceed 1.5 tend to be surgically repaired, while those below this threshold tend to be managed medically.[23,24] This is in large part because more severe shunts predispose patients to pulmonary hypertension due to the excess pulmonary flow.

Role of MRI in Congenital Heart Disease

Magnetic resonance imaging has a multifaceted role in the management of patients with congenital heart disease. Imaging, whether by echocardiography, CT, or MRI, is essential in the initial diagnosis, reassessment of diagnosis and surgical intervention upon transfer of care, and in long-term follow-up for detection of complications. Although echocardiography remains a first line modality for initial assessment, MRI has become routine in the management of many congenital conditions largely because of its ability to visualize structures that remain obscured with echocardiography, without ionizing radiation. At present, some of the most commonly encountered entities in clinical practice include the entities described above (repaired tetralogy of Fallot, aortic coarctation, and partial anomalous pulmonary venous return), as well as many other conditions. In each of these circumstances, there are structures of interest for which complete visualization is necessary for adequate evaluation.

MRI further provides quantitative data of blood flow and ventricular function that provide reliable means for longitudinal follow-up. The conventional approach to cardiac MRI in the setting of CHD involves a lengthy iterative set of sequences to determine blood flow and cardiac function and to delineate the relevant anatomy. This typically requires acquisition times on the order of one hour, and requires supervision by an experienced cardiac imager to ensure that images are obtained in the correct plane and location with proper selection of imaging parameters in real-time, while the patient is still in the magnet.

The 4D flow is an MRI method that yields both a vector of blood velocity as well as magnitude signal intensity over an imaging volume, such as the whole chest, for each temporal phase of the cardiac cycle. With this single acquisition, MRI simultaneously addresses each of the primary components of the imaging evaluation of congenital heart disease, which can be largely classified as: (i) quantification of blood flow, (ii) quantification of ventricular volumes and function, and (iii) visualization of intracardiac and extracardiac structures and blood flow. With a highly spatially and temporally resolved technique, 4D flow can obtain these data in a manner that improves upon the techniques which are currently prevalent (Table 1). First, rather than rely on prescription of multiple planes at each valve or structure of interest to obtain assessment of net and regurgitant flow, as is currently the case with conventional phase-contrast imaging, planes are prescribed retrospectively at each valve of interest without any incremental cost in imaging time. Second, rather than rely on a stack of 8- to 10-mm-thick cine steady-state images to evaluate myocardial function, short-axis or long-axis cine images of the heart can be retrospectively reconstructed from 4D flow images. Third, rather than rely on a separate MRA for anatomic delineation of extracardiac structures, 4D flow can provide both anatomic visualization and superimposition of flow data to localize significant stenoses or collateral vessels. As acquisition and image reconstruction strategies for 4D flow continue to evolve, the ability to accomplish each of these tasks with this single pulse sequence should become increasingly routine.

4D Flow Data Acquisition

Phase-Contrast Imaging

Phase contrast imaging uses the complex nature of the MRI signal to obtain accurate quantitative velocity measurements. This is possible because any applied gradient $\vec{G}$ will affect the phase of a group of moving spins. It can be shown that the phase of the acquired MR signal can be written as[25]:

$$\phi(t)=\phi_0(\vec{r})+\vec{r}_0\cdot\gamma\overrightarrow{M}_0+\vec{v}_0\cdot\gamma\overrightarrow{M}_1+\frac{1}{2}\vec{a}_0\cdot\gamma\overrightarrow{M}_2+\ldots,$$

where the gradient moment $\overrightarrow{M_i}$ is defined as:

$$\overrightarrow{M_i}=\int_0^t t'^i\,\vec{G}(t')dt'.$$

Velocity encoding in a particular direction is typically done using a set of gradients that are designed to have a net area of zero. Because $\overrightarrow{M_0}=0$ these gradients are often referred to as a bipolar pair. If the acceleration and higher order terms are ignored, the phase due to the application of the bipolar gradient is dependent on the spin velocity $\vec{v}_0$ as:

$$\varphi(t)=\varphi_0(\vec{r})+\vec{v}_0\cdot\gamma\vec{M}_1,$$

where $\overrightarrow{M_1}$ is the first moment of the bipolar pair. Because the Fourier transform resolves signal amplitudes and phases as functions of spatial location, the phase in each pixel can be measured.

It is important to note that the measured phase has contributions from sources other than the application of the bipolar gradient alone. The phase term φ_0 is voxel dependent and arises from a variety of sources, such as B_0 inhomogeneity, susceptibility differences, off-resonance effects, eddy currents, and RF inhomogeneity.[26] As a result, resolution of the flow in one direction requires the use of two acquisitions with different gradient $\overrightarrow{M_1}$ values. If these acquisitions are denoted as S_1 and S_2, and the total change in first moment is $\Delta\overrightarrow{M_1}$, then it can be shown that a phase map can be created by taking the phase difference at each point in the image[27]:

$$I_{\Delta\phi}=\arg(S_2/S_1)$$

where $\arg(S_i)$ is the phase of the complex signal S_i. Finally, an apparent velocity image can be created using the magnitude of the bipolar first moment:

$$I_v=I_{\Delta v}/\gamma\Delta M_1.$$

This type of imaging is referred to as phase contrast (PC) imaging.[28,29]

An important parameter in acquiring a phase contrast image is the velocity encoding value, or VENC. The VENC value is defined as the velocity that produces a phase shift of π radians, or:

$$VENC=\pi/\gamma\Delta M_1.$$

It can be seen that including sign information, unambiguous velocity measurements can only be made for phase shifts between $\pm\pi$. Therefore, some knowledge of the velocities being imaged must be used to avoid velocity aliasing in the reconstructed images. Typically the VENC is set to be slightly greater than the largest velocities expected. In

TABLE 1. 4D-Flow MRI Studies in Congenital Heart Disease

Reference	Year	Patients (n)	Field strength (Tesla)	Acceleration type	Acceleration factor		Sampling resolution		Temporal resolution (ms)	Venc	Scan time (min)	Conclusion
					In-Plane	Slice	In-Plane	Slice				
Westenberg, et al[64]	2008	20	1.5T	EPI	5	-	1.4	4	10% window	150	-	4D flow accurate for mitral and tricuspid valve flow quantification, even in patients with regurgitation.
van der Hulst, et al[69]	2010	25	1.5T	EPI	5	-	1.4	4	10% window	>150	-	4D flow accurate for quantification of pulmonary and tricuspid valve flow.
Geiger, et al [70]	2011	10	1.5T/3T	PI	2	-	-	-	37.6–40.8	150–200	-	4D flow feasible for comprehensive blood flow evaluation in CHD.
Hsiao, et al [63]	2011	18	1.5T	PI	2x outer	-	1.15 (0.86-1.84)	3.89 (3–5)	35.9 (33–42)	258 (150–400)	(15) 9–21	4D flow has greater precision in flow quantification than 2D-PC.
Francois et al [71]	2012	11	1.5T/3T	PC VIPR	-	-	1.02-1.25	1.02-1.25	35–44/ 25–27	40–400	9–17	PC VIPR 4D flow enables detection of right heart flow patterns in repaired TOF.
Hsiao, et al[47]	2012	14 (2009)	1.5T	PI	2x outer	-	1.63 (1.15-2.34)	3.53 (3–4)	37 (29–64)	270 (150–500)	9:32 (4–15)	PI-CS 4D flow magnitude images can be adequate for ventricular volumetry.
Hsiao, et al[47]	2012	15 (2010)	1.5T	PI-CS	1.6-2.2	1.6-2.2	1.13 (0.78-1.67)	2.51 (2–3.4)	64 (33–86)	223 (150–300)	9:30 (7–15)	PI-CS 4D flow blood flow measurements match volumetry better than 2D-PC.

TABLE 1: Continued

Reference	Year	Patients (n)	Field strength (Tesla)	Acceleration type	Acceleration factor		Sampling resolution		Temporal resolution (ms)	Venc	Scan time (min)	Conclusion
					In-Plane	Slice	In-Plane	Slice				
Hsiao, et al[68]	2012	34	1.5T	PI-CS	1.4-2.2	1.4-2.2	1.02 (0.78-1.82)	2.30 (1.2–3.4)	61 (31–86)	(120–350)	9:43 (5–15)	PI-CS 4D flow adequate for visualization of shunts and hemodynamically significant valve regurgitation.
Markl, et al [72]	2012	1	1.5T	PI	2	-	1.8x2.3	2.8	41	150	15	Potential role of 4D flow for follow-up of patients with complex cardiovascular anatomy.
Valverde, et al[73]	2012	29	1.5T	PI	2	-	1.5	2.3	-	150–400	12:34 ± 03:42	4D flow reliable in assessment of systemic-to-pulmonary collateral flow.
Tariq, et al [55]	2013	22	1.5T	PI-CS	2-2.2	2-2.2	1.11	-	53	231 (150–350)	10:44 (6:46-14:58)	PI-CS 4D flow at high Venc (250+) is adequate for venous flow quantification.
Hanneman, et al[74]	2014	19	1.5T	GRAPPA	2	-	2.4	3	46 + nav delay	150	18.75±4.58	4D flow comparable to 2D-PC for Qp:Qs for intra-cardiac shunts.
Hsiao, et al[66]	2014	34	1.5T	PI-CS	1.6-2.2	1.6-2.2	1.21 (0.78-1.88)	2.39 (2–3.4)	61 (33–86)	222 (120–350)	10:10 (6:46-14:58)	PI-CS 4D flow alone accurate for quantification of regurgitant volume and fraction.

Averages are provided with ranges in parentheses where appropriate. EPI = echo planar imaging; PI = parallel imaging; PI-CS = parallel imaging compressed sensing; VIPR = isotropic-voxel radial projection imaging; TOF = Tetralogy of Fallot.

periodic flows such as blood flow in the human arterial system, the velocities vary significantly throughout the cardiac cycle. To improve the measurement accuracy, Ringgaard et al implemented a sequence in which variable VENCs are tailored to the different phases of the cardiac cycle.[30]

Because measuring flow in one direction requires two acquisitions to remove any baseline phase contributions, the obvious extension for multiple flow directions is to keep adding pairs of acquisitions for each axis. However, aside from the extra cost in imaging time (six repetition times [TRs] would be necessary to measure flow along all three directions) the redundancy in the baseline measurement is unnecessary. Instead, the measurement of multiple flow directions can use a single common measurement to remove baseline phase. A common configuration for measuring flow in all directions is the "simple four-point" method,[31] in which the flow-encoding value is alternated in each TR. If it is assumed that the complex signal S_i has equal and uncorrelated noise in each channel with variance σ^2, and that each measurement S_i has comparable signal ($|S_i| \approx |S|$, for all i), it can be shown that the variance in the velocity image can be written as[32]:

$$\sigma_v^2 = (2\sigma^2 VENC^2)/|\pi S|^2.$$

This equation shows that the noise in a phase contrast image is dependent on the local signal strength but is independent of the measured phase. Furthermore, the noise will increase linearly as the VENC increases. Therefore, the optimal PC acquisition will incorporate a large enough VENC to prevent aliasing, but not one so large as to unnecessarily increase the image noise. It is possible to collect data with an artificially low VENC and then un-wrap the aliased velocity data using a second scan performed with an appropriate VENC (33). This approach takes advantage of the higher velocity-to-noise ratio of the low VENC scan at the cost of extra imaging time.

Time-Resolved Flow Imaging

Historically PC-MRI acquisitions have tended to be lengthy, and as such have had difficulty being incorporated in regular clinical practice. Scan times are anywhere from two to four times longer than a corresponding non-PC based study, and because in vivo flow is not constant, accurate measurements are only possible with gated sequences. Gating makes it possible to produce a series of cine images showing the flow dynamics over the cardiac cycle, but to do so more time must be spent repeating the acquisition to resolve the temporal dynamics. Finally, the weaker gradient amplitudes of early systems led to longer sequence repetition times, which in turn limited the achievable temporal resolution.

Early acquisitions were based on gated 2D sequences that primarily measured through-plane flow.[29,34] Either prospective or retrospective gating could be used to trigger data collection at the beginning of each cardiac cycle. Generally, the total number of needed in-plane *k*-space locations, N_{ky}, would be divided up into groups (or segments), and each segment would be repeatedly sampled over the course of the R–R interval until the subsequent trigger would start the acquisition of the next segment. The number of phase encodes in each segment can be denoted as Nseg, and to measure a single direction of flow it is necessary to repeat the acquisition of each phase encode location twice. Therefore, the temporal resolution of the scan is given by $T_{res} = 2 \times TR \times N_{seg}$, and the total scan time, in heartbeats, is given by N_{ky}/N_{seg}. At the end of the study the data collected during a particular temporal window could be used to produce an image of the flow at that phase of the cardiac cycle. For example, given a moderate resolution of 128 N_{ky} locations and a typical segmentation of $N_{seg} = 8$, 16 heartbeats would be needed to complete a study which could be done in a single breath-hold. If each TR had a length of 15 ms, this would produce a set of CINE images with a temporal resolution of 240 ms.

The extension to 3D imaging was straightforward, but given the limitations of early systems the resulting scan times were prohibitively long. As with 2D, the common approach to 4D flow MRI would divide up the total number N_k of (k_y,k_z) *k*-space acquisitions into N_{seg} segments that are repeatedly sampled during one R–R interval (Fig. 3). Because four measurements are needed for three flow directions, the resulting temporal resolution of the data is given as:

$$T_{res} = 4 \times TR \times N_{seg}$$

while the number of R–R intervals needed to complete the scan is then:

$$N_{RR} = N_k / N_{seg}.$$

Early efforts by Wigström et al[35] produced a sequence using a TR of 21 ms that was capable of imaging a 16 slice volume with a spatial resolution of (0.94 × 1.9 × 3.8) mm^3 in 23 min. Here the 16 slices were divided into eight 2 segment groups, producing a temporal resolution of 168 ms. The practical development of 4D-Flow acquisitions were made possible by several developments. Stronger gradient systems resulted in shorter sequence TRs that allowed the collection of more *k*-space lines in each segment. In addition, the introduction of contrast agents made it possible to recover the signal that was lost as a result of the more frequent excitation. Work by Tyszka used a 10.5 ms TR to image a 16 slice volume with a spatial resolution of (2.5 × 2.5 × 3) mm^3 in approximately 13 min. The 16 slices were divided into 16 groups of 1 segment each to produce a temporal resolution of 42 ms.[36] Markl et al were able to use

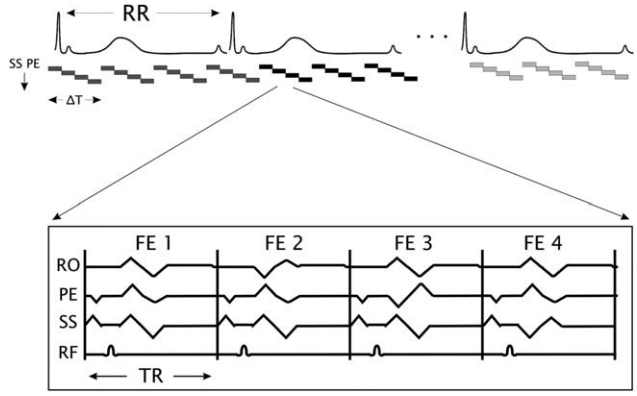

FIGURE 3: Schematic showing the acquisition pattern for 4D-Flow MRI. Within each RR interval, a group of $N_{seg} = 4$ (ky,kz) pairs are repeatedly sampled (shown here as sets of 4 solid blocks). Each block consists of four different TRs in which the individual flow encodings are acquired. The temporal resolution of the data, denoted here as ΔT, is then given as $4*TR*N_{seg}$.

fractional echo techniques to achieve TRs on the order of 5 ms, which produced scan times of 12–18 min for volumes with spatial resolutions on the order of $(1.25 \times 2 \times 4)$ mm^3.[37]

While the operator does have the ability to trade off an increase in temporal resolution for a decrease in scan time, as shown by the two equations above, clinically useful spatial and temporal resolutions require scan times that are in the range of 10–20 min for fully sampled acquisitions. Unlike in 2D multi-slice imaging, breath-holding is clearly not possible.

Simple respiratory compensation can be done by selecting an appropriate set of (k_y,k_z) phase encodes based on the phase of the respiratory cycle at the instant of the R–R trigger, which is termed respiratory ordered phase encoding, or ROPE.[38] In the best case the effect is a set of images that appear to have been acquired over a single long breath. While this technique tends to produce only moderate image quality improvements, no extra scan time is needed.

Navigator gating generally produces better image quality by rejecting data that are acquired outside of an acceptance window that is usually based on diaphragm position.[39–41] Because this technique does not require respiratory bellows, it has the added advantage of greater patient acceptance. However, any data that are rejected must be reacquired at the cost of an increase in scan time. Work by Markl et al has attempted to mitigate this by increasing the acceptance width while dynamically repositioning the window based on movement of the diaphragm.[42] This approach can also be used together with ROPE to determine which set of phase encodes will be acquired when in the window so that any remaining artifacts can be minimized. Another approach to increase navigator efficiency is to only gate at the center of *k*-space.[43] This requires only minimal increases in scan times with no degradation in measured flow values.

Aside from potentially increasing scan times, navigators can be problematic in that any time spent acquiring navigator data is time not spent measuring flow. One approach to solving this issue is the use of self-gating techniques to measure *k*-space profiles motion at regular, shorter intervals during the study.[44] Data acceptance can then be based on motion estimates derived from the correlation of measured and reference profiles.

Faster Approaches to Acquisition

Even though 4D flow techniques have been in development for almost two decades, it is still not a technique with wide clinical acceptance. As discussed above, respiration artifacts can produce poor image quality. Also, a successful exam can produce thousands of images that can be overwhelming to process. However, the single greatest impediment to widespread clinical adoption has been the long scan times that are necessary. This has started to change with the development of various approaches to undersampling data, to the point where routine clinical scans can be completed in 10 min or less.

The most straight-forward approach to reducing scan times is to use a basic parallel imaging technique such as GRAPPA to reduce the number of phase encode sets that need to be acquired.[45] With the development of compressed sensing reconstructions in conjunction with pseudo-random sampling patterns such as variable density Poisson disk, the number of needed phase-encode sets can be further reduced.[46,47] While in all cases the practical amount of reduction depends on the coil geometry and number of elements, compressed sensing reconstructions will generally tolerate larger reduction factors than when using parallel imaging alone.[48] Our institution typically uses overall compressed sensing reduction factors of 9–11 to image volumes with $(1.3 \times 1.6 \times 2.6)$ mm^3 in approximately 5 min, and sub-millimeter in-plane resolutions of $(0.8 \times 0.8 \times 2.6)$ mm^3 in approximately 9 min.

Parallel imaging techniques provide scan time reductions by reducing the number of phase encode sets that are needed for each cardiac phase. Even greater scan time reductions can be realized by exploiting the spatio-temporal correlation inherent in the dynamic data. Methods such as *k-t* BLAST and *k-t* SENSE can achieve five- to eightfold increases in acceleration by varying the undersampled sampling pattern from phase to phase.[49,50]

Finally, non-Cartesian acquisitions such as spiral and radial can exploit their increased sampling efficiency to reduce scan times and improve resolution[51,52] (Fig. 4). Three-dimensional radial sampling is advantageous in that it can provide spherical isotropic resolution at the millimeter level in scan times on the order of 7–12 min.[53,54] Non-Cartesian applications are prone to aliasing issues from objects larger than the in-plane field of view (FOV), but

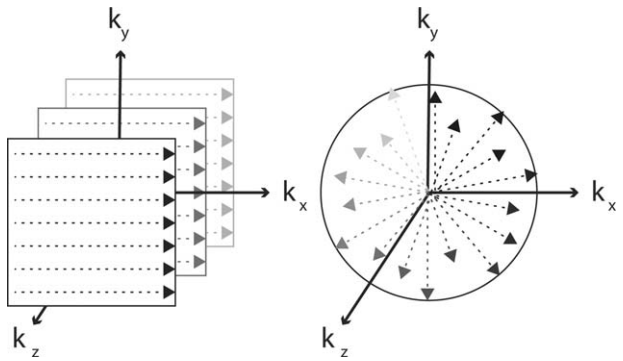

FIGURE 4: A simplified representation illustrating some differences between Cartesian and radial sampling. In Cartesian sampling (left), each TR acquires a set of points along k_x at one (k_y, k_z) location. Here each acquisition starts on the left and moves toward the right in the direction of the arrow. In radial sampling (right), which is used in PC-VIPR, each TR acquires data in along a spoke that starts at the center of *k*-space and moves outward along a different (k_x,k_y,k_z) path each time.

unlike in Cartesian sampling the resulting artifacts are less structured and more benign in appearance.

Scan prescription

Although our current protocols continue to evolve, in our experience, the most important factor to enabling comprehensive assessment of flow, function, and anatomy with 4D flow is acquisition of data with adequate spatial and temporal resolution. A conservative starting point is a matrix of 256 × 192 with 2.5 mm slices interpolated to 1.25 mm slices; with a FOV covering the whole chest and temporal resolution of 60 ms for heart rates below 80 and 40 ms for faster heart rates, comprehensive analysis is feasible. There are several approaches to selection of venc. Although a low resolution high-venc acquisition can be obtained as a venc scout, we find this impractical. Instead, a venc of 250 cm/s is used. With this venc, we have always been able to find a slice through arteries that has no aliasing and have been able to preserve accuracy of low velocity veins.[55] Though phase-unwrapping may enable determination of peak velocities, the accuracy and reliability of this approach has not been established. However, in our practice, estimation of peak velocities has been of secondary importance. Our current protocol used in daily practice leverages a blood pool contrast agent, provides 320 × 320 matrix and 1.6 mm slices interpolated to 0.8 mm, with temporal resolution of approximately 50 ms. With this resolution, we have found ventricular segmentation and anatomic analysis to be easier and more confidently performed with 4D flow than conventional cine and MRA imaging.

4D Flow data correction

At the foundation of MRI is the use of weak linear gradients to perform spatial encoding. In practice most gradients can only produce truly linear gradients over a small volume at the center of the coil, and as a result the reconstructed images will contain nonlinear distortions that increase with distance from the isocenter of the magnet. Depending on the gradient coil, gradient strengths can deviate by more than 60% over a 40 cm^3 volume.[56] This problem can be corrected with postprocessing algorithms that are part of the standard reconstruction software packages.[57] However, it should be noted that this correction often is not done in the slice direction for either multi-slice 2D or volumetric 3D data acquisitions.

The nonlinearity of the imaging gradients also has consequences for flow measurements. Because of this distortion there can be significant deviations between the intended and actual flow encodings that will affect the magnitude and direction of the encoded velocities.[56] Angular deviations can be as much as 13° at the edge of a 20 cm^3 volume and 45° at the edge of a 40 cm^3 volume. One can predict these 3D deviations with knowledge of the gradient coil profile, and this information can then be used to fully correct 3D velocity data. If only one-directional flow is measured through the slice plane, the distortion causes the local slice-select gradient to be parallel to the local flow encoding direction, and a magnitude correction of the velocity data can be shown to be sufficient.

Anytime a gradient is activated, additional nonlinear gradients appear as a result of Maxwell's conditions that the divergence of the field is zero and the curl of the field is negligible. To lowest order, these additional gradients produce field components that are nonlinear and inversely proportional to the main field strength B_0.[58] Because PC-MRI depends on the difference of at least two acquisitions with different gradient configurations, the result is that these so-called Maxwell terms will introduce shading into the reconstructed phase images. These phase effects can be corrected using a postprocessing correction as part of the image reconstruction. It can be shown that four coefficients are necessary to calculate the induced Maxwell phase as a function of spatial location. These terms depend on the strength and timing of the imaging gradients; therefore, these terms can be easily calculated by the sequence before each scan for later use in the reconstruction.

Gradient activity during scanning also induces eddy currents in the magnet. Eddy currents appear as small amplitude residual gradients of opposite polarity that decay exponentially and are present in all MR scans.[59] Unlike the Maxwell phase effects, which are a function of gradient amplitude, eddy currents depend on the slew rate of the applied gradients. In phase contrast imaging, residual eddy currents will produce a spatially varying background phase that is mostly linear and is characterized by one or more exponential decay time constants.[60,61] While most commercial systems reduce these effects by using pre-emphasis filters to shape the gradients, it is common to find residual phase

offsets that will affect quantitative measurements. Because eddy current effects are system specific, this residual background error must be removed using postprocessing algorithms. For in vivo research, the most common approach is to measure phase in the static background areas surrounding the flow, and then use the measurements to estimate the phase correction throughout the image.[62]

Interpretation Techniques

Velocity Data Interpretation

Routine measurement of blood flow in cardiovascular MRI can be generally classified into two main tasks: (i) quantification of stenoses and (ii) quantification of bulk flow (including net, forward and regurgitant flow). The first, quantification of stenosis, provides an assessment of the hemodynamic significance of a given anatomic narrowing and relies on the peak of the velocity profile for a vessel of interest. The second, quantification of bulk flow, relies on integration of the velocity profile across a particular cross-section of a vessel.

By conventional 2D phase contrast imaging, evaluation of a suspected stenosis currently requires precise positioning of a plane at the location of peak velocity, oriented orthogonal to the direction of flow. Proper selection of this plane can require multiple oblique localizers and considerable experience to perform. The peak velocity is then used to estimate the pressure gradient associated with the flow acceleration. The modified Bernoulli-equation, $\Delta P \approx 4v^2$, is then used to estimate the pressure gradient (ΔP, in mmHg) based on the peak velocity, (v, in m/s). While its assumptions are relatively crude, including assumptions of steady-state and nonpulsatile flow, this equation has been used routinely in practice to stratify adult patients requiring surgical intervention for aortic valve surgery based on echocardiographic peak velocities.

MRI is the only modality that can simultaneously reliably visualize the relevant anatomy and measure velocity in patients with aortic coarctation (Fig. 5). It is often challenging by conventional imaging to precisely identify the peak velocity spatially, because the greatest measured velocity can lie at some distance distal to the site of maximum anatomic narrowing. Some cardiac imagers have advocated for in-plane mapping of the velocity profile to help identify the true peak, albeit at the cost of increasing scan time and necessitating special expertise at the scanner. With 4D flow MRI, it is possible to measure the entire velocity field for the thoracic aorta and identify the peak retrospectively. It remains to be determined, however, whether this approach truly provides more accurate measurements of the gradient than conventional MRI.

Quantification of bulk flow with conventional 2D phase contrast imaging is similarly challenging, particularly near stenoses or regurgitant valves. The altered hemodynamics

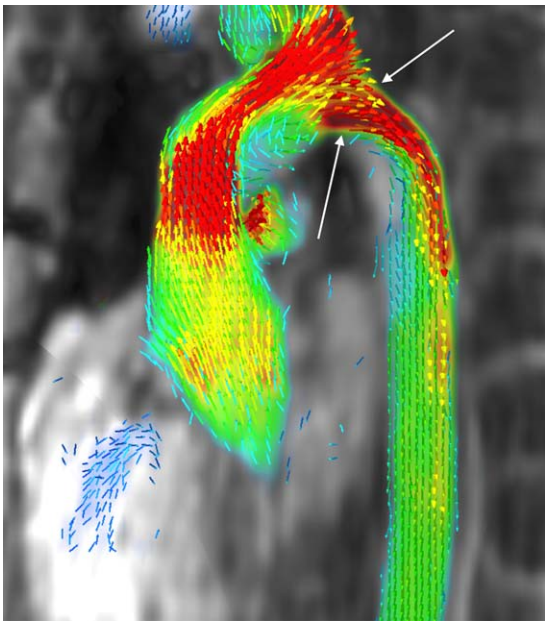

FIGURE 5: The 4D flow acquisition of a 14-year-old boy with repaired aortic coarctation, now with residual stenosis of the distal aortic arch. Note coverage of the entire thoracic aorta. Peak velocity was measured at 1.9 m/s and peak gradient was estimated at 14 mmHg based on the modified Bernoulli equation. The mild degree of residual stenosis and absence of any aneurysm meant that further repair was not immediately necessary. Total acquisition time for the 4D flow was 12:11.

near stenosis and regurgitation are known to impair the accuracy of the phase-contrast technique. Under-resolved spatial acceleration, temporal acceleration, and turbulence have each been proposed to impair the accuracy of phase-contrast. Thus, to obtain accurate bulk flow measurements using conventional imaging, an experienced cardiac imager will need to obtain multiple cut planes at and near a stenotic and/or regurgitant valve, oriented orthogonal to each of the forward or regurgitant jets. Furthermore, respiratory artifact and surgical devices such as coils, metallic valves, and sternal wires can partially obscure structures of interest. After obtaining each of these measurements, the cardiac imager then needs to apply his or her experience to resolve discrepancies in the resultant data.

Using 4D flow, a cardiac imager computationally obtains the appropriate reformatted imaging planes retrospectively from the imaging volume (Fig. 6). Thus, instead of relying on clinical experience at the time of image-acquisition, he or she can apply knowledge of the factors that impact accurate flow quantification at the postprocessing workstation, particularly with postprocessing software for 4D flow that enables efficient user-interactive plane selection. Because the factors that impact flow quantification are similar between conventional phase-contrast and 4D flow, experience with conventional imaging can inform proper selection of planes. In our experience in the clinical setting, bulk flow measurements by 4D flow tend to be less prone to error than conventional phase-contrast. Specifically,

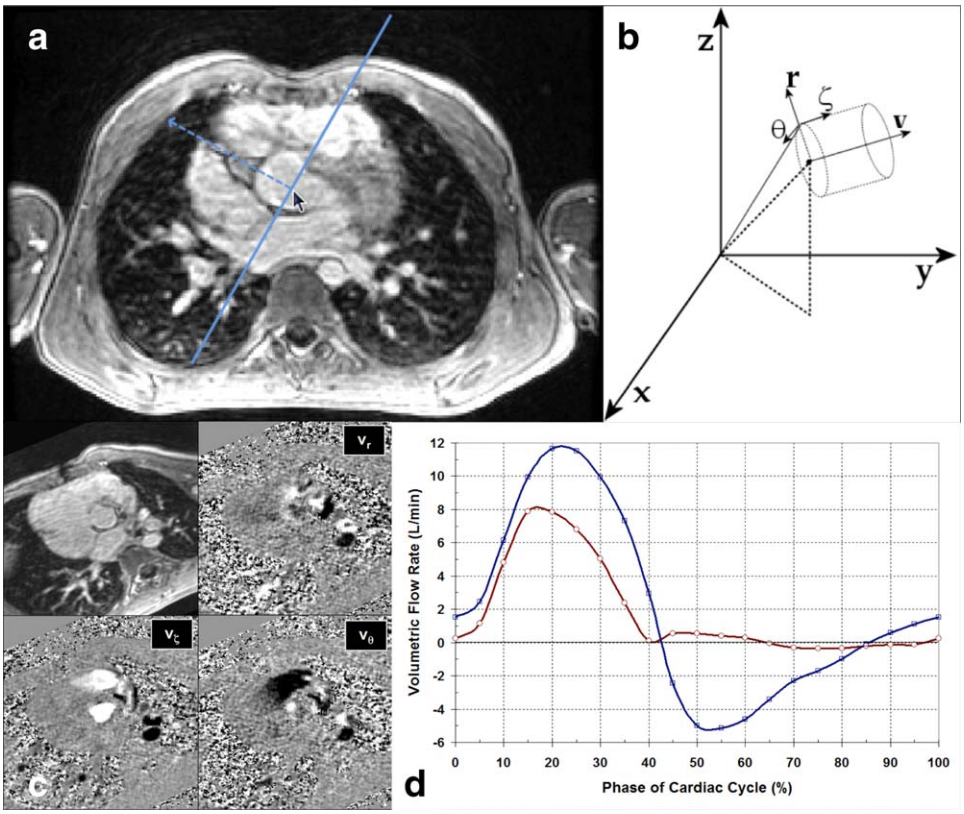

FIGURE 6: Approach to obtaining bulk flow in arbitrary structures. a: Once a structure of interest is found, such as the aorta (b), the plane perpendicular to the direction of flow in the vessel can be obtained (b). c: In that plane velocity be represented in cylindrical coordinates. d: Once a structure is segmented velocity in the through plane component can be summed for each voxel in the segmentation, yielding a curve of flow over the cardiac cycle. Here the red curve shows aortic flow, whereas the blue curve shows pulmonary regurgitation (corresponding plane not shown).

aortic and pulmonary flow measurements by conventional phase-contrast can be rather discrepant in the absence of shunts, but to a significantly lesser extent by 4D flow.[63] These bulk flow measurements also correlate better with displacements of ventricular volume than conventional phase-contrast.[47]

In the case of partial anomalous pulmonary venous return, the severity of pulmonary-to-systemic shunting helps to determine the need for surgical intervention. Anatomic mapping (described below) further helps localize the morphology of the pulmonary venous shunts, and determine the approach to surgical repair (Fig. 7).

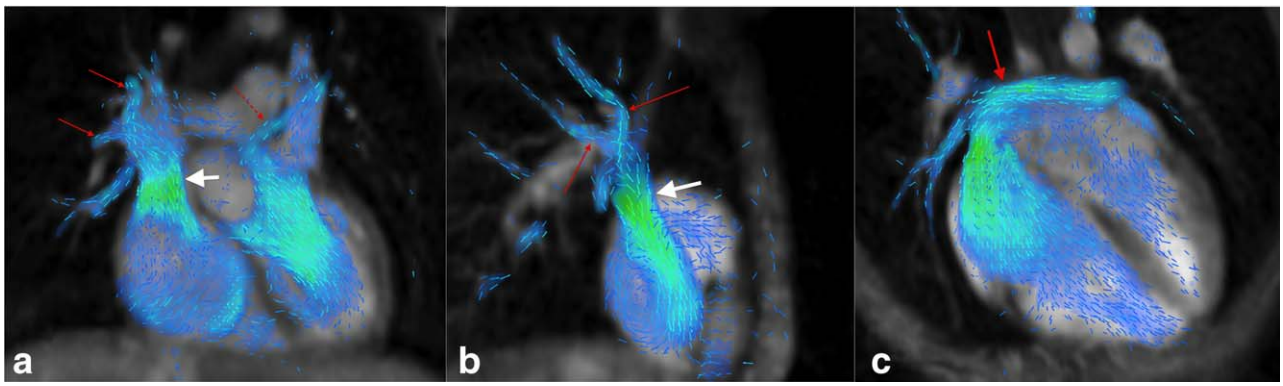

FIGURE 7: A 13-year-old boy with partial anomalous pulmonary venous return and a sinus venosus ASD. Coronal (a) and sagittal (b) views show anomalous right upper pulmonary veins (red arrows) draining to the superior vena cava (white arrow). c: Oblique four-chamber view shows flow from the left atrium crossing into the right atrium through the atrial septal defect (arrow). Pulmonary arterial flow (Q_p) was measured using methods shown in Figure 6 at 6.84 L/min, while systemic arterial flow (Q_s) was measured at 3.35 L/min, resulting in a shunt fraction (Q_p/Q_s) of 2.04. Incidentally, the sinus venosus shunt measured 1.60 L/min, comprising 46% of the right-to-left shunt volume. Total acquisition time for the 4D flow was 10 min, 22 s.

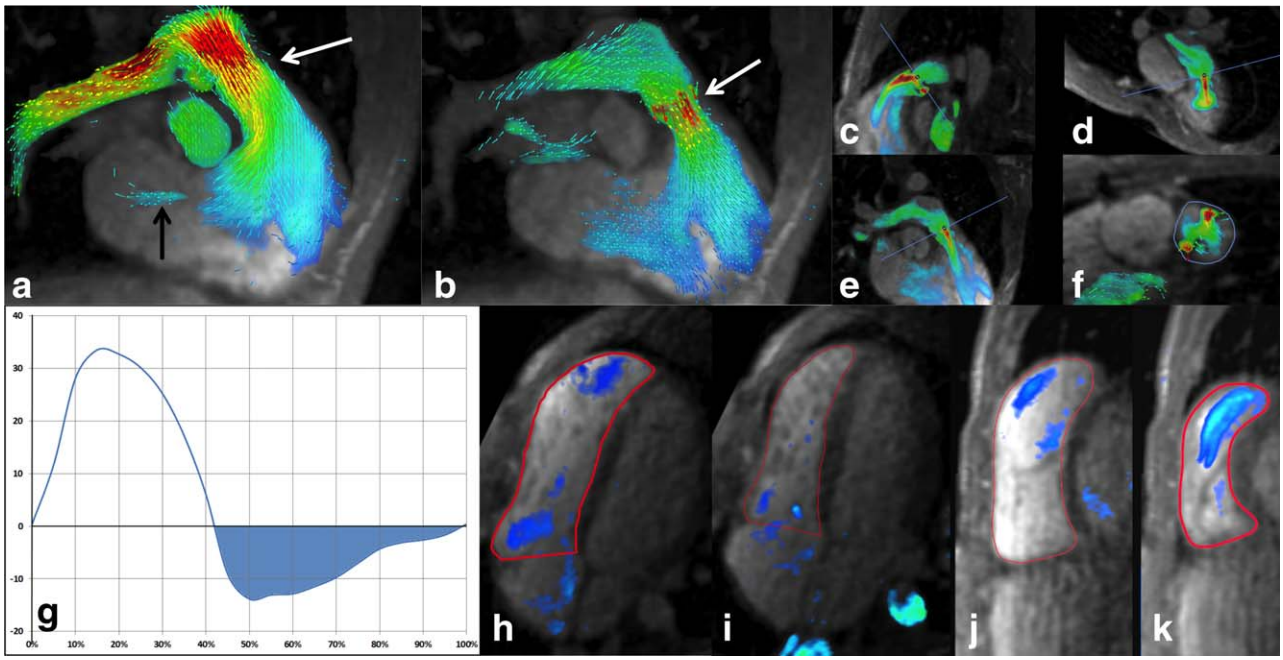

FIGURE 8: A 15-year-old boy with tetralogy of Fallot after repair. a: Systolic image show high velocities in the pulmonary artery (white arrow), indicative of pulmonic stenosis and a jet of tricuspid regurgitation (black arrow). b: Diastolic image shows pulmonic regurgitation as well (arrow). Multi-planar reformations (c–f) allow optimal segmentation of pulmonary artery yield a flow curve (g) for calculation of regurgitant fraction of 48%. Magnitude data can be reformatted in the long axis in both diastole (h) and systole (i), and segmentation of the right ventricle performed to determine ventricular volume and ejection fraction. Alternatively, reformats can be obtained in the traditional short axis plane (j,k). Total acquisition time for the 4D flow was 7 min, 29 s.

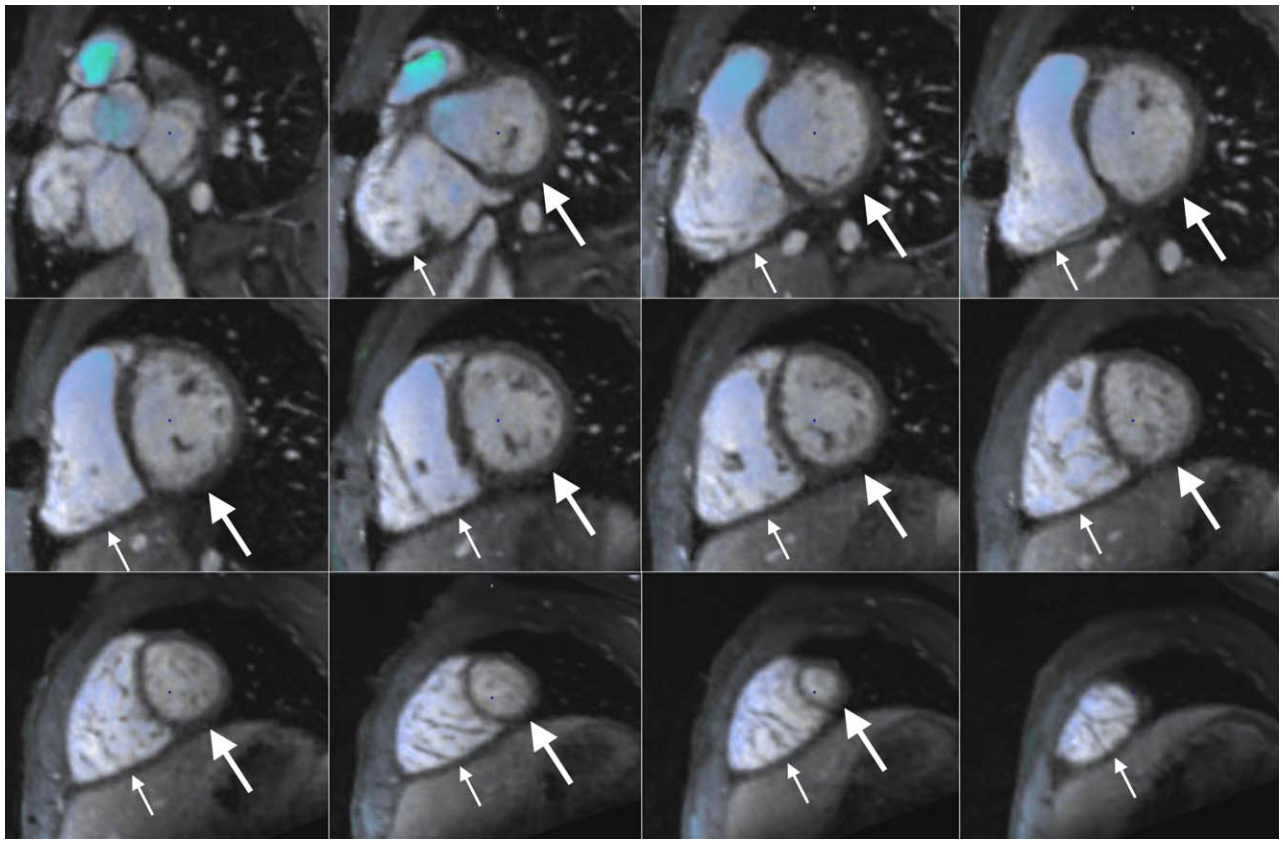

FIGURE 9: Stack of diastolic phase images reformatted to short axis plane covering from base of the heart to the apex. Left (thick arrows) and right (thin arrows) ventricles can easily be segmented.

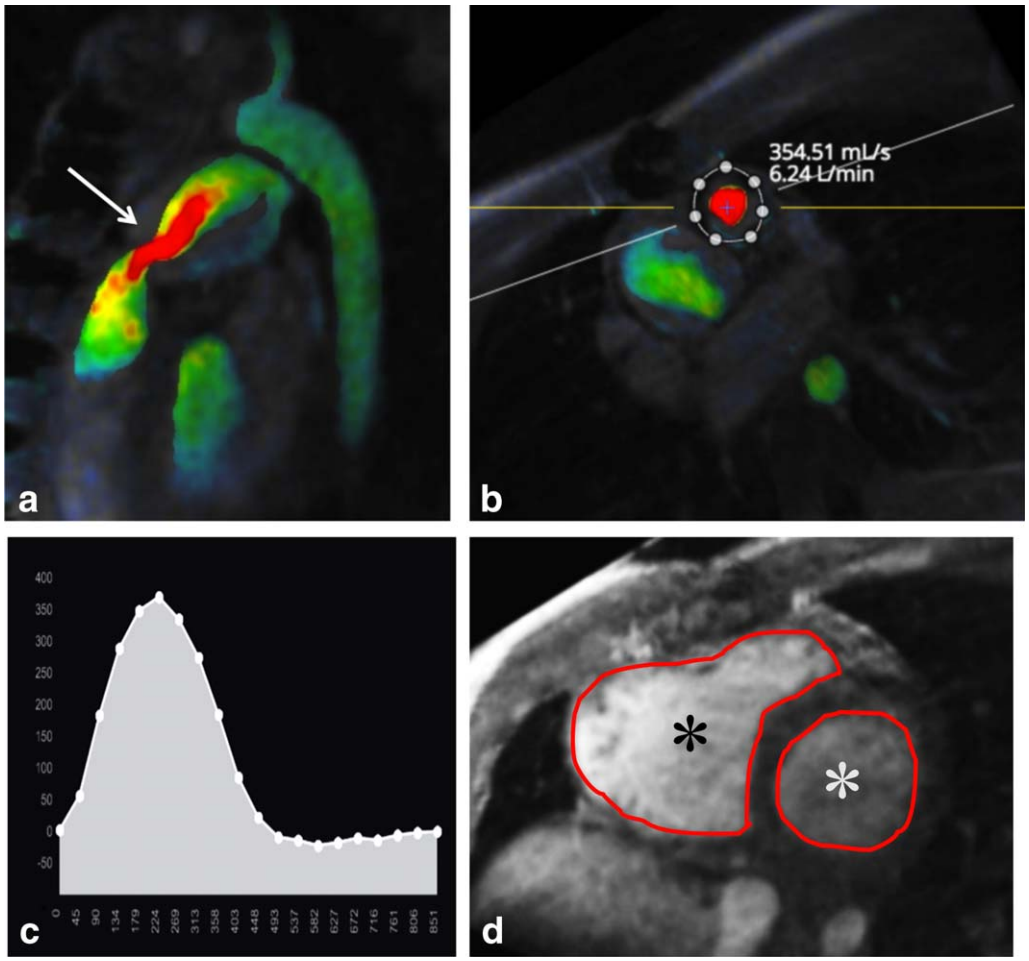

FIGURE 10: A 20-year-old female with tetralogy of Fallot, after repair. a: Significant flow acceleration was noted across the pulmonary conduit (arrow). Peak velocity at the conduit was measured at 2.1 m/s and peak gradient was estimated at 17 mmHg based on the modified Bernoulli equation. b: Reformat to plane perpendicular to direction of pulmonary artery flow permits segmentation of the vessel. c: The resulting flow curve yields a mild pulmonary regurgitant fraction of 4%. d: Gray scale images reformatted into the short axis plane are used to quantify right (black asterisk) and left (white asterisk) ventricular volumes and ejection fraction. These confirmed right ventricular enlargement.

Another potential advantage of 4D flow is the ability to prescribe dynamic planes for quantification of blood flow. For example, because the mitral and tricuspid valves and regurgitant jets may translate significantly during the course of the cardiac cycle, and are difficult to accurately assess with static imaging planes, whether by echocardiography or conventional MRI. Some groups have applied a strategy of dynamic plane prescription based on separate short and long-axis steady-state free-precession (SSFP) acquisitions, which seem to work reasonably well.[64,65] Alternatively, we have found that these conventional SSFP acquisitions may not be necessary when high image-quality 4D flow acquisitions are obtained. It is possible to prescribe a dynamic plane from the simultaneously acquired anatomic data, and provide estimates of net and regurgitant volume that better correlate with ventricular blood displacements than conventional imaging.[66]

As noted previously, accurate quantification of regurgitant volume can inform the need for and timing of surgical repair (Fig. 8). For example, in patients with tetralogy of Fallot or congenital pulmonary stenosis, many patients experience chronic pulmonary regurgitation and right ventricular volume loading as a consequence of the surgical or interventional repair. When chronic regurgitation is long-standing, a subset of these patients can eventually develop right ventricular failure. The severity of pulmonary regurgitation in these patients helps provide a biomarker and predictor of the onset of failure. For example, a patient with mild regurgitation (regurgitant fraction $<20\%$) is much less likely to develop right ventricular failure than a similar patient with severe regurgitation (regurgitant fraction $>40\%$). The severity of regurgitation can thus be used to suggest shorter interval follow-up in patients who do not undergo immediate repair of the regurgitant valve.

Magnitude Cine Data Interpretation: Ventricular Volumes and Function

Conventional planar SSFP imaging has long been the standard technique for assessment of myocardial function by

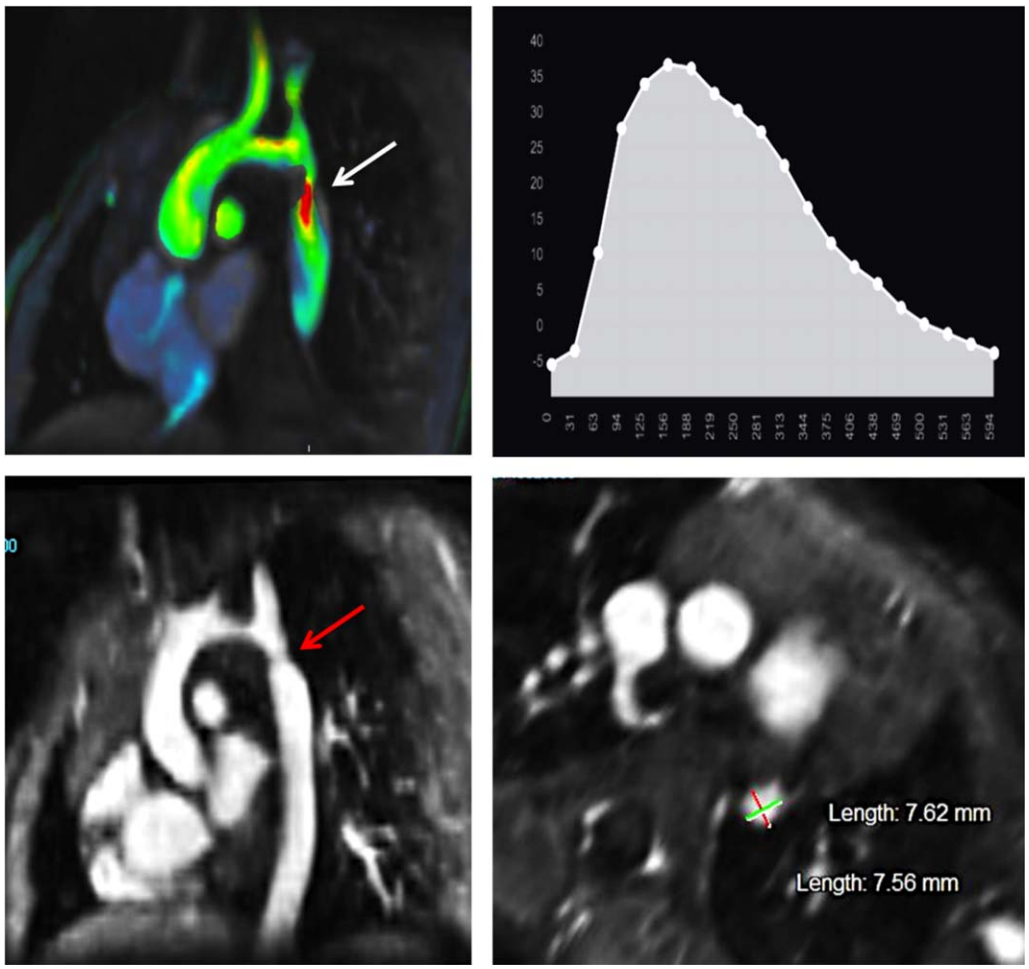

FIGURE 11: A 4-year-old boy with aortic coarctation. There is significant flow acceleration across the coarctation (arrow, top left). Peak velocity was measured at 1.9 m/s and peak gradient was estimated at 15 mmHg based on the modified Bernoulli equation. Gray scale 4D flow magnitude images are important to evaluate the relevant anatomy (arrow, oblique sagittal bottom left, and cross-section bottom right). The cross-sectional diameter of the coarctation measured 7 × 8 mm.

MRI. It has a distinct advantage of achieving high signal-to-noise and high contrast distinction between blood pool and myocardium without the need to administer intravenous contrast. However, relatively thick 8–10 mm slices are typically used. To achieve the sharpest demarcation of blood pool and myocardium, optimal SSFP imaging requires a series of breath holds. Unfortunately, these images may not necessarily be registered with respect to each other due to inconsistencies in breath hold position. Furthermore, because breath holds can by themselves alter cardiac physiology, affecting venous return and cardiac output, breath holds have also been partly blamed for inconsistencies between volumetric flow rates and ventricular blood displacements.

Volumetric cardiac MRI with 4D flow may help to resolve some of these issues by providing a mechanism to analyze myocardial function in its averaged state over multiple respiratory and cardiac cycles. With a low echo time SPGR-technique, off-resonance effects and signal void artifacts from surgical material are much less problematic than with SSFP imaging, especially when imaging is performed at 3T. Retrospective reformatting of the volumetric cine data (Fig. 9) into a stack of short-axis images permits segmentation of the ventricles in systole and diastole to extract venricular volumes and ejection fractions.

One of the challenges of obtaining accurate segmentations of ventricles with 4D flow is relatively low signal to noise and blood pool-myocardial contrast. Although velocity images may aid in segmentation, in practice administration of intravenous contrast solves this dilemma. For most congenital diseases, delayed enhancement imaging is not required, and thus a blood pool contrast agent may be administered. In situations where delayed enhancement is required, a protocol of injection of an extracellular contrast agent to obtain myocardial perfusion imaging is followed by 4D flow acquisition, and then delayed enhancement imaging. With use of acceleration strategies, the 4D flow scan can be completed in approximately 5 min, which is then the ideal time to begin acquiring delayed enhancement images. We have found that with this strategy of volumetric imaging, it is increasingly possible to use anatomic data from 4D flow to obtain equivalent estimates of ventricular

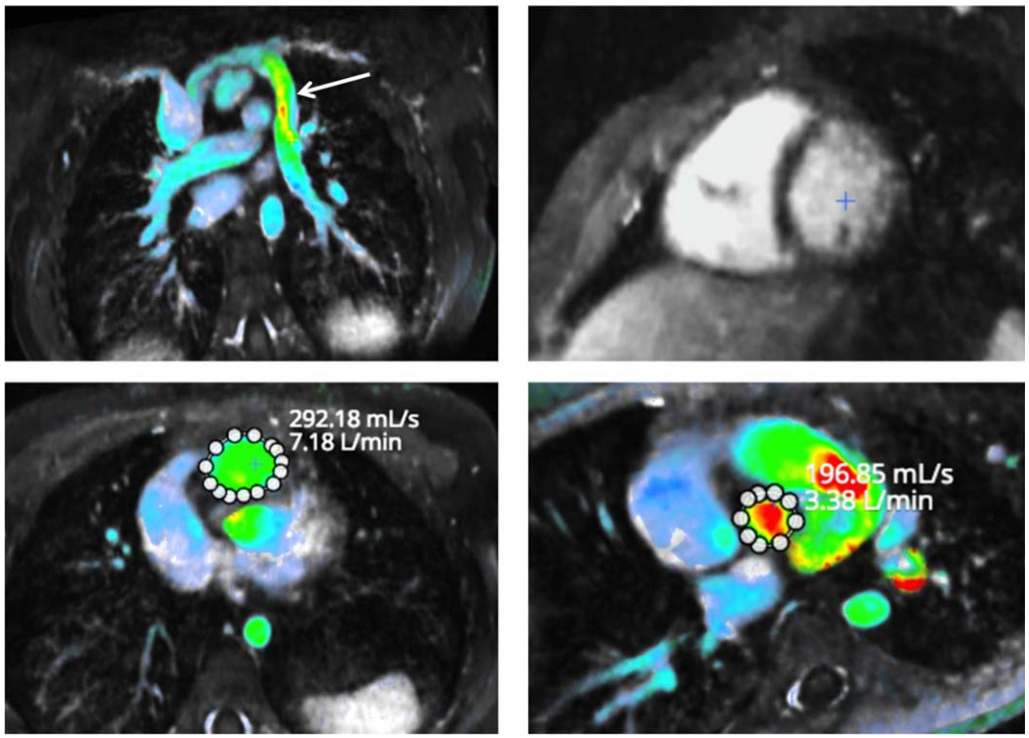

FIGURE 12: A 7-year-old girl with partial anomalous pulmonary venous return. All pulmonary flow from the left lung returned to right atrium instead of the left atrium. Oblique coronal (top left) views show anomalous pulmonary venous drainage from the left lung to a large vertical vein (arrow). This anomalous vein connects to the left brachiocephalic vein, draining into the right-sided superior vena cava. All pulmonary flow from the right lung returned to the left atrium. Gray scale images are used to quantify ventricular volumes and function, notably right ventricular end-diastolic volume and ejection fraction (short axis image in end-diastole, top right). By these volumes, right sided stroke volume was more than double the left. Pulmonary arterial flow (Q_p) was measured at 7.18 L/min (bottom left), while systemic arterial flow (Q_s) was measured at 3.38 L/min (bottom right), resulting in a shunt ratio (Q_p/Q_s) of 2.12).

volume and ejection fraction to those routinely obtained by breath-held short-axis SSFP.[47,67]

In the example of patients with tetralogy of Fallot, volumetry has a very critical role in prognostication and decision-making for planning repair of the pulmonary valve. It is now widely accepted that when right ventricular dilatation is sufficiently severe, irreversible remodeling of the right ventricle can take place where repair of the pulmonary valve is no longer effective to recover right ventricular function.

Visualization and Segmental Analysis

Visualization of the intracardiac and extracardiac structures and blood flow is an essential component of the cardiac MRI examination for congenital heart disease. Current clinical practice is directed at anatomic visualization with precisely placed imaging planes, tailored to the patient's underlying congenital heart defects and the clinical questions at hand. For example, the imaging planes required for evaluation of repaired tetralogy of Fallot are different from the imaging planes needed for coarctation or anomalous pulmonary venous drainage. Due to time-constraints, conventional MRI visualization of blood flow is limited to the very few imaging planes that are explicitly prescribed at the time of the examination.

4D flow provides yet another opportunity to resolve a current limitation to the current practice of congenital heart MRI. It is possible now to cover the entire anatomic region of interest—the entire chest—and complete the scan in a clinically feasible time. All of the anatomic structures and the entire flow field can be captured in this comprehensive scan. This includes intracardiac structures for identification of leaks in surgical baffles or patches as well as extracardiac structures for localization of occult shunts like collaterals or anomalous pulmonary veins. The morphology and severity of leaks from incompetent valves can also be readily characterized with visualization that exceeds current practice in cardiac MRI.[68]

Software platforms for the above analyses include EnSight (Apex, NC), Arterys, Inc. (San Francisco, CA), and Gyrotools GTFlow (Zurich).

Examples of 4D Flow Evaluation in CHD

The 4D flow MRI Evaluation provides critical information in patients with congenital heart disease, including repaired TOF, aortic coarctation and PAPVR as examples. In the setting of rTOF, 4D flow MRI assessment includes evaluation and quantification of pulmonary regurgitation, quantification of velocity and pressure gradient across the pulmonary valve in the setting of residual or recurrent pulmonary stenosis, and evaluation of right ventricular size and function (Fig. 10). In patients with coarctation of the aorta, 4D flow

MRI evaluation provides both anatomic and hemodynamic information, including characterization of the location and size of the coarcted segment, and quantification of the peak velocity and pressure gradient across the stenosis (Fig. 11). In the setting of PAPVR, 4D flow MRI provides critical anatomic information including characterization of pulmonary venous drainage from all pulmonary segments. Accurate quantification of pulmonary (Q_P) and systemic (Q_S) arterial flow, with calculation of the shunt fraction (Q_P/Q_S), as well as evaluation of ventricular size and function, is imperative in the pre-operative evaluation of patients with a left-to-right shunt, including PAPVR (Fig. 12).

In conclusion, evaluation of congenital heart disease requires assessments of flow, function, and anatomy. Historically this has required a lengthy MRI protocol with iterative skilled prescription of scan planes. The 4D flow provides a comprehensive assessment of congenital heart disease in a single acquisition that requires little user skill. Ongoing efforts are directed toward decreasing scan time further and mitigating motion artifacts. Tools for postprocessing 4D flow for practical interpretation in the clinic are becoming more widely available and will facilitate wider usage of the technique.

References

1. Hoffman J, Kaplan S. The incidence of congenital heart disease. J Am Coll Cardiol 2002;39:1890–1900.
2. Van Praagh R. The segmental approach to diagnosis in congenital heart disease. Birth Defects 1972;8:4–23.
3. Go AS, Mozaffarian D, Roger VL, et al. Executive summary: heart disease and stroke statistics–2014 update: a report from the American Heart Association. Circulation 2014;129:399–410.
4. Pillutla P, Shetty KD, Foster E. Mortality associated with adult congenital heart disease: trends in the US population from 1979 to 2005. Am Heart J 2009;158:874–879.
5. Al Habib HF, Jacobs JP, Mavroudis C, et al. Contemporary patterns of Management of Tetralogy of Fallot: data from The Society of Thoracic Surgeons Database. Ann Thorac Surg 2010;90:813–820.
6. Karl T. Tetralogy of Fallot: current surgical perspective. Ann Pediatr Cardiol 2008;1:93.
7. Geva T. Repaired tetralogy of Fallot: the roles of cardiovascular magnetic resonance in evaluating pathophysiology and for pulmonary valve replacement decision support. J Cardiovasc Magn Reson 2011;13:9.
8. Geva T, Sandweiss BM, Gauvreau K, Lock JE, Powell AJ. Factors associated with impaired clinical status in long-term survivors of tetralogy of Fallot repair evaluated by magnetic resonance imaging. J Am Coll Cardiol 2004;43:1068–1074.
9. Oosterhof T, Mulder BJM, Vliegen HW, de Roos A. Cardiovascular magnetic resonance in the follow-up of patients with corrected tetralogy of Fallot: a review. Am Heart J 2006;151:265–272.
10. Davlouros PA, Kilner PJ, Hornung TS, et al. Right ventricular function in adults with repaired tetralogy of Fallot assessed with cardiovascular magnetic resonance imaging: detrimental role of right ventricular outflow aneurysms or akinesia and adverse right-to-left ventricular interaction. J Am Coll Cardiol 2002;40:2044–2052.
11. Kenny D, Hijazi ZM. Coarctation of the aorta: from fetal life to adulthood. Cardiol J 2011;18:487–495.
12. Brown ML, Burkhart HM, Connolly HM, et al. Coarctation of the aorta: lifelong surveillance is mandatory following surgical repair. J Am Coll Cardiol 2013;62:1020–1025.
13. Cohen M, Fuster V, Steele PM, Driscoll D, McGoon DC. Coarctation of the aorta. Long-term follow-up and prediction of outcome after surgical correction. Circulation 1989;80:840–845.
14. Hamdan MA, Maheshwari S, Fahey JT, Hellenbrand WE. Endovascular stents for coarctation of the aorta: initial results and intermediate-term follow-up. J Am Coll Cardiol 2001;38:1518–1523.
15. Celermajer DS, Greaves K. Survivors of coarctation repair: fixed but not cured. Heart 2002;88:113–114.
16. Presbitero P, Demarie D, Villani M, et al. Long term results (15–30 years) of surgical repair of aortic coarctation. Heart 1987;57:462–467.
17. Shih M-CP, Tholpady A, Kramer CM, Sydnor MK, Hagspiel KD. Surgical and endovascular repair of aortic coarctation: normal findings and appearance of complications on CT angiography and MR angiography. AJR Am J Roentgenol 2006;187:W302–W312.
18. Hope MD, Meadows AK, Hope TA, et al. Clinical evaluation of aortic coarctation with 4D flow MR imaging. J Magn Reson Imaging 2010; 31:711–718.
19. Holmqvist C, Ståhlberg F, Hanséus K, et al. Collateral flow in coarctation of the aorta with magnetic resonance velocity mapping: correlation to morphological imaging of collateral vessels. J Magn Reson Imaging 2002;15:39–46.
20. Demos TC, Posniak HV, Pierce KL, Olson MC, Muscato M. Venous anomalies of the thorax. AJR Am J Roentgenol 2004;182:1139–1150.
21. Yong MS, d'Udekem Y, Robertson T, et al. Outcomes of surgery for simple total anomalous pulmonary venous drainage in neonates. Ann Thorac Surg 2011;91:1921–1927.
22. Robinson BL, Kwong RY, Varma PK, Wolfe M, Couper G. Magnetic resonance imaging of complex partial anomalous pulmonary venous return in adults. Circulation 2014;129:e1–e2.
23. Warnes CA, Williams RG, Bashore TM, et al. ACC/AHA 2008 guidelines for the management of adults with congenital heart disease: executive summary: a report of the American College of Cardiology/American Heart Association Task Force on Practice Guidelines (writing committee to develop guidelines for the management of adults with congenital heart disease). Circulation 2008:2395–2451.
24. Silversides CK, Dore A, Poirier N, et al. Canadian Cardiovascular Society 2009 Consensus Conference on the management of adults with congenital heart disease: shunt lesions. Can J Cardiol 2010;26:e70–e79.
25. Elkins CJ, Alley MT. Magnetic resonance velocimetry: applications of magnetic resonance imaging in the measurement of fluid motion. Exp Fluids 2007;43:823–858.
26. Pelc NJ. Flow quantification and analysis methods. Magn Reson Imaging Clin North Am 1995;3:413–424.
27. Pelc NJ, Bernstein MA, Shimakawa A. Encoding strategies for three-direction phase-contrast MR imaging of flow. J Magn Reson Imaging 1991;1:405–413.
28. Dumoulin CL, Souza SP, Walker MF, Wagle W. Three-dimensional phase contrast angiography. Magn Reson Med 1989;9:139–149.
29. Pelc NJ, Herfkens RJ, Shimakawa A, Enzmann DR. Phase contrast cine magnetic resonance imaging. Magn Reson Q 1991;7:229–254.
30. Ringgaard S, Oyre SA, Pedersen EM. Arterial MR imaging phase-contrast flow measurement: improvements with varying velocity sensitivity during cardiac cycle. Radiology 2004;232:289–294.
31. Pelc NJ, Bernstein MA, Shimakawa A, Glover GH. Encoding strategies for three-direction phase-contrast MR imaging of flow. J Magn Reson Imaging 1991;1:405–413.
32. Conturo TE, Smith GD. Signal-to-noise in phase angle reconstruction: dynamic range extension using phase reference offsets. Magn Reson Med 1990;15:420–437.
33. Lee AT, Pike GB, Pelc NJ. Three-point phase-contrast velocity measurements with increased velocity-to-noise ratio. Magn Reson Med 1995;33:122–126.
34. Glover GH, Pelc NJ. A rapid-gated cine MRI technique In: Kressel HY, editor. Magnetic resonance annual 1988. New York: Raven; 1988. p 299–333.

35. Wigström L, Sjöqvist L, Wranne B. Temporally resolved 3D phase-contrast imaging. Magn Reson Med 1996;36:800–803.

36. Tyszka JM, Laidlaw DH, Asa JW, Silverman JM. Three-dimensional, time-resolved (4D) relative pressure mapping using magnetic resonance imaging. J Magn Reson Imaging 2000;12:321–329.

37. Markl M, Chan FP, Alley MT, et al. Time-resolved three-dimensional phase-contrast MRI. J Magn Reson Imaging 2003;17:499–506.

38. Bailes DR, Gilderdale DJ, Bydder GM, Collins AG, Firmin DN. Respiratory ordered phase encoding (ROPE): a method for reducing respiratory motion artefacts in MR imaging. J Comput Assist Tomogr 1985;9:835–838.

39. Ehman RL, Felmlee JP. Adaptive technique for high-definition MR imaging of moving structures. Radiology 1989;173:255–263.

40. Firmin D, Keegan J. Navigator echoes in cardiac magnetic resonance. J Cardiovasc Magn Reson 2001;3:183–193.

41. Baltes C, Kozerke S, Atkinson D, Boesiger P. Retrospective respiratory motion correction for navigated cine velocity mapping. J Cardiovasc Magn Reson 2004;6:785–792.

42. Markl M, Harloff A, Bley TA, et al. Time-resolved 3D MR velocity mapping at 3T: improved navigator-gated assessment of vascular anatomy and blood flow. J Magn Reson Imaging 2007;25:824–831.

43. Akçakaya M, Gulaka P, Basha TA, Ngo LH, Manning WJ, Nezafat R. Free-breathing phase contrast MRI with near 100% respiratory navigator efficiency using k-space-dependent respiratory gating. Magn Reson Med 2014;71:2172–2179.

44. Uribe S, Beerbaum P, Sørensen TS, Rasmusson A, Razavi R, Schaeffter T. Four-dimensional (4D) flow of the whole heart and great vessels using real-time respiratory self-gating. Magn Reson Med 2009;62:984–992.

45. Bammer R, Hope TA, Aksoy M, Alley MT. Time-resolved 3D quantitative flow MRI of the major intracranial vessels: initial experience and comparative evaluation at 1.5T and 3.0T in combination with parallel imaging. Magn Reson Med 2007;57:127–140.

46. Lustig M, Donoho D, Pauly JM. Sparse MRI: the application of compressed sensing for rapid MR imaging. Magn Reson Med 2007;58: 1182–1195.

47. Hsiao A, Lustig M, Alley MT, et al. Rapid pediatric cardiac assessment of flow and ventricular volume with compressed sensing parallel imaging volumetric cine phase-contrast MRI. AJR Am J Roentgenol 2012; 198:W250–W259.

48. Vasanawala SS, Alley MT, Hargreaves BA, Barth RA, Pauly JM, Lustig M. Improved pediatric MR imaging with compressed sensing. Radiology 2010;256:607–616.

49. Baltes C, Kozerke S, Hansen MS, Pruessmann KP, Tsao J, Boesiger P. Accelerating cine phase-contrast flow measurements using k-t BLAST and k-t SENSE. Magn Reson Med 2005;54:1430–1438.

50. Jung B, Stalder AF, Bauer S, Markl M. On the undersampling strategies to accelerate time-resolved 3D imaging using k-t-GRAPPA. Magn Reson Med 2011;66:966–975.

51. Gu T, Korosec FR, Block WF, et al. PC VIPR: a high-speed 3D phase-contrast method for flow quantification and high-resolution angiography. AJNR Am J Neuroradiol 2005;26:743–749.

52. Sigfridsson A, Petersson S, Carlhäll C-J, Ebbers T. Four-dimensional flow MRI using spiral acquisition. Magn Reson Med 2012;68:1065–1073.

53. Frydrychowicz A, Landgraf BR, Niespodzany E, et al. Four-dimensional velocity mapping of the hepatic and splanchnic vasculature with radial sampling at 3 tesla: a feasibility study in portal hypertension. J Magn Reson Imaging 2011;34:577–584.

54. Frydrychowicz A, Landgraf B, Wieben O, François CJ. Images in cardiovascular medicine. Scimitar syndrome: added value by isotropic flow-sensitive four-dimensional magnetic resonance imaging with PC-VIPR (phase-contrast vastly undersampled isotropic projection reconstruction). Circulation 2010;121:e434–e436.

55. Tariq U, Hsiao A, Alley M, Zhang T, Lustig M, Vasanawala SS. Venous and arterial flow quantification are equally accurate and precise with parallel imaging compressed sensing 4D phase contrast MRI. J Magn Reson Imaging 2013;37:1419–1426.

56. Markl M, Bammer R, Alley MT, et al. Generalized reconstruction of phase contrast MRI: analysis and correction of the effect of gradient field distortions. Magn Reson Med 2003;50:791–801.

57. Glover GH, Pelc NJ. Method for correcting image distortion due to gradient nonuniformity. US Patent Office; U.S. patent number 4591789, 1986.

58. Bernstein MA, Zhou XJ, Polzin JA, et al. Concomitant gradient terms in phase contrast MR: analysis and correction. Magn Reson Med 1998;39:300–308.

59. Ahn CB, Cho ZH. Analysis of eddy currents in nuclear magnetic resonance imaging. Magn Reson Med 1991;17:149–163.

60. Glover GH, Pelc NJ, Bradshaw KM. Gradient and polarizing field compensation. US Patent Office; U.S. patent number 4950994, 1990.

61. Glover GH, Pelc NJ. Method for magnetic field gradient eddy current compensation. US Patent Office; U.S. patent number 4698591, 1987.

62. Walker PG, Cranney GB, Scheidegger MB, Waseleski G, Pohost GM, Yoganathan AP. Semiautomated method for noise reduction and background phase error correction in MR phase velocity data. J Magn Reson Imaging 1993;3:521–530.

63. Hsiao A, Alley MT, Massaband P, Herfkens RJ, Chan FP, Vasanawala SS. Improved cardiovascular flow quantification with time-resolved volumetric phase-contrast MRI. Pediatr Radiol 2011;41:711–720.

64. Westenberg JJM, Roes SD, Ajmone Marsan N, et al. Mitral valve and tricuspid valve blood flow: accurate quantification with 3D velocity-encoded MR imaging with retrospective valve tracking. Radiology 2008;249:792–800.

65. Roes SD, Hammer S, van der Geest RJ, et al. Flow assessment through four heart valves simultaneously using 3-dimensional 3-directional velocity-encoded magnetic resonance imaging with retrospective valve tracking in healthy volunteers and patients with valvular regurgitation. Invest Radiol 2009;44:669–675.

66. Hsiao A, Tariq U, Alley MT, Lustig M, Vasanawala SS. Inlet and outlet valve flow and regurgitant volume may be directly and reliably quantified with accelerated, volumetric phase-contrast MRI. J Magn Reson Imaging 2014. [Epub ahead of print].

67. Roldan-Alzate A, Frydrychowicz A, Johnson KM, et al. Non-invasive assessment of cardiac function and pulmonary vascular resistance in an canine model of acute thromboembolic pulmonary hypertension using 4D flow cardiovascular magnetic resonance. J Cardiovasc Magn Reson 2014;16:23.

68. Hsiao A, Lustig M, Alley MT, Murphy MJ, Vasanawala SS. Evaluation of valvular insufficiency and shunts with parallel-imaging compressed-sensing 4D phase-contrast MR imaging with stereoscopic 3D velocity-fusion volume-rendered visualization. Radiology 2012;265:87–95.

69. van der Hulst AE, Westenberg JJM, Kroft LJM, et al. Tetralogy of fallot: 3D velocity-encoded MR imaging for evaluation of right ventricular valve flow and diastolic function in patients after correction. Radiology 2010;256:724–734.

70. Geiger J, Markl M, Jung B, et al. 4D-MR flow analysis in patients after repair for tetralogy of Fallot. Eur Radiol 2011;21:1651–1657.

71. François CJ, Srinivasan S, Schiebler ML, et al. 4D cardiovascular magnetic resonance velocity mapping of alterations of right heart flow patterns and main pulmonary artery hemodynamics in tetralogy of Fallot. J Cardiovasc Magn Reson 2012;14:16.

72. Markl M, Geiger J, Jung B, Hirtler D, Arnold R. Noninvasive evaluation of 3D hemodynamics in a complex case of single ventricle physiology. J Magn Reson Imaging 2012;35:933–937.

73. Valverde I, Nordmeyer S, Uribe S, et al. Systemic-to-pulmonary collateral flow in patients with palliated univentricular heart physiology: measurement using cardiovascular magnetic resonance 4D velocity acquisition. J Cardiovasc Magn Reson 2012;14:25.

74. Hanneman K, Sivagnanam M, Nguyen ET, et al. Magnetic resonance assessment of pulmonary (QP) to systemic (QS) flows using 4D phase-contrast imaging: pilot study comparison with standard through-plane 2D phase-contrast imaging. Acad Radiol 2014;21:1002–1008.